Search for a dark leptophilic scalar produced in association with $\tau^+\tau^-$ pair in e^+e^- annihilation at center-of-mass energies near 10.58 GeV

D. Biswas, Sw. Banerjee, I. Adachi, H. Aihara, D. M. Asner, T. Aushev, R. Ayad, V. Babu, P. Behera, J. Bennett, M. Bessner, V. Bhardwaj, B. Bhuyan, T. Bilka, D. Bodrov, J. Borah, A. Bozek, M. Bračko, P. Branchini, T. E. Browder, A. Budano, M. Campajola, D. Červenkov, M.-C. Chang, P. Chang, B. G. Cheon, K. Chilikin, H. E. Cho, K. Cho, S.-K. Choi, Y. Choi, S. Choudhury, D. Cinabro, S. Das, G. De Nardo, G. De Pietro, R. Dhamija, F. Di Capua, J. Dingfelder, Z. Doležal, T. V. Dong, S. Dubey, P. Ecker, D. Epifanov, T. Ferber, B. G. Fulsom, V. Gaur, A. Garmash, A. Giri, P. Goldenzweig, E. Graziani, Y. Guan, K. Gudkova, C. Hadjivasiliou, K. Hayasaka, H. Hayashii, S. Hazra, M. T. Hedges, D. Herrmann, M. Hernández Villanueva, W.-S. Hou, C.-L. Hsu, K. Inami, G. Inguglia, N. Ipsita, A. Ishikawa, R. Itoh, M. Iwasaki, W. W. Jacobs, Q. P. Ji, S. Jia, Y. Jin, K. K. Joo, A. B. Kaliyar, C. Kiesling, C. H. Kim, D. Y. Kim, K.-H. Kim, Y. J. Kim, Y.-K. Kim, P. Kodyš, T. Konno, A. Korobov, S. Korpar, P. Križan, P. Krokovny, M. Kumar, K. Kumara, Y.-J. Kwon, Y.-T. Lai, M. Laurenza, S. C. Lee, D. Levit, J. Li, L. K. Li, Y. Li, L. Li Gioi, J. Libby, K. Lieret, Y.-R. Lin, D. Liventsev, T. Luo, Y. Ma, M. Masuda, S. K. Maurya, F. Meier, M. Merola, F. Metzner, K. Miyabayashi, R. Mizuk, I. Nakamura, M. Nakao, Z. Natkaniec, A. Natochii, L. Nayak, M. Niiyama, N. K. Nisar, S. Nishida, S. Ogawa, H. Ono, P. Pakhlov, G. Pakhlova, S. Pardi, H. Park, J. Park, S.-H. Park, A. Passeri, S. Patra, S. Paul, R. Pestotnik, L. E. Piilonen, T. Podobnik, E. Prencipe, M. T. Prim, N. Rout, G. Russo, S. Sandilya, L. Santelj, V. Savinov, G. Schnell, C. Schwanda, Y. Seino, K. Senyo, M. E. Sevior, W. Shan, C. Sharma, J.-G. Shiu, B. Shwartz, J. B. Singh, A. Sokolov, E. Solovieva, M. Starič, Z. S. Stottler, M. Sumihama, M. Takizawa, K. Tanida, F. Tenchini, K. Trabelsi, M. Uchida, T. Uglov, Y. Unno, K. Uno, S. Uno, P. Urquijo, A. Vinokurova, D. Wang, E. Wang, S. Watanuki, E. Won, X. Xu, B. D. Yabsley, W. Yan, J. H. Yin, C. Z. Yuan, L. Yuan, Z. P. Zhang, V. Zhilich, V. Zhukova, and V. Zhulanov

(Belle Collaboration)

A dark leptophilic scalar (ϕ_L) is a hypothetical particle that couples only to leptons rather than quarks. We report on a search for ϕ_L in the $e^+e^- \to \tau^+\tau^-\phi_L, \phi_L \to \ell^+\ell^- (\ell = e, \mu)$ process using 626 fb^{-1} of data collected by the Belle experiment near the $\Upsilon(4S)$ resonance. We validate the backgrounds with multiple control regions in data, using a novel multiclass multivariate event classifier. In absence of a signal, we quote upper limits at the 90% confidence level on the coupling between ϕ_L and leptons. Our bounds, obtained in a blinded approach, are 19% more constraining than the previous limits, averaged over the mass range $0.04 \leq m_{\phi_L} \leq 6.5$ GeV. We exclude the parameter space below 4 GeV favored by measurement of the anomalous magnetic moment of the muon.

The astrophysical observation of the dark matter in the Universe [1], and measured excess over Standard Model (SM) expectations in the anomalous magnetic moment of the muon, $(g-2)_\mu$ [2], could be signatures of new physics beyond the SM. Recently, models with a dark leptophilic scalar (ϕ_L), which couples directly only to leptons [3,4], have been introduced at mass scales substantially lighter than the weak scale. Models, in which a generic dark scalar (ϕ) couples to quarks as well, are strongly constrained by the existing limits on the decays through flavor-changing neutral current, such as $B \to K\phi$ and $K \to \pi\phi$ [5,6]. The leptophilic models evade most of such existing bounds with a minimal scenario that includes a mixing between ϕ_L and the SM particles [7,8]. These models can explain the observed excess in measured $(g-2)_\mu$ [9–11], violation of lepton flavor universality [12,13], or recent hints of new physics in a model-independent framework [14].

In this model, mixing between ϕ_L and the Higgs boson produces couplings proportional to fermion masses, described by the following term in the Lagrangian [10]:

$$\mathcal{L} = -\xi \sum_{\ell=e,\mu,\tau} \frac{m_\ell}{v} \overline{\ell} \phi_L \ell, \qquad (1)$$

where ξ denotes the strength of flavor-independent coupling to leptons (ℓ) with mass m_ℓ, and $v = 246$ GeV [15] is the vacuum expectation value of the Higgs field.

Here, we report a search for a leptophilic scalar in the process $e^+e^- \to \tau^+\tau^-\phi_L$, $\phi_L \to \ell^+\ell^-(\ell = e, \mu)$. The dominant Feynman diagram is shown in Fig. 1.

The cross section of $e^+e^- \to \tau^+\tau^-\phi_L$, $\phi_L \to e^+e^-$ falls sharply beyond the dimuon threshold, where the $\phi_L \to \mu^+\mu^-$ channel opens up [10]. We search in $\phi_L \to e^+e^-$ channel only up to ϕ_L mass $m_{\phi_L} = 2m_\mu$, and $\phi_L \to \mu^+\mu^-$ channel for $m_{\phi_L} > 2m_\mu$. Although for $m_{\phi_L} > 2m_\tau$, the cross section of the $e^+e^- \to \tau^+\tau^-\phi_L$, $\phi_L \to \mu^+\mu^-$ process decreases [10], we are still able to set competitive limits till $m_{\phi_L} = 6.5$ GeV.

The data used in this analysis was recorded by the Belle experiment from the collision of 8 GeV electrons with 3.5 GeV positrons at the KEKB collider [16]. The Belle detector, a large-solid-angle magnetic spectrometer, is described in detail elsewhere [17]. Outward from 15 mm radius beam pipe [18], it consists of a four-layer silicon vertex detector, a 50-layer central drift chamber (CDC), an array of aerogel threshold Cherenkov counters (ACC), a barrel-like arrangement of time-of-flight scintillation counters, and an electromagnetic calorimeter comprised of CsI (Tl) crystals (ECL), all located inside a superconducting solenoid coil that provides a 1.5 T magnetic field. Clean electron identification is obtained by combining the responses of the ECL, CDC, and ACC detectors, while muons are identified by CDC and resistive plate chambers in the instrumented iron flux-return located outside the coil.

The data-set corresponds to a luminosity of 626 fb^{-1} collected after the upgrade of the silicon vertex detector subdetector in October 2003. Out of these, 562 fb^{-1} was collected at the $\Upsilon(4S)$ resonance and the remaining at a c.m.
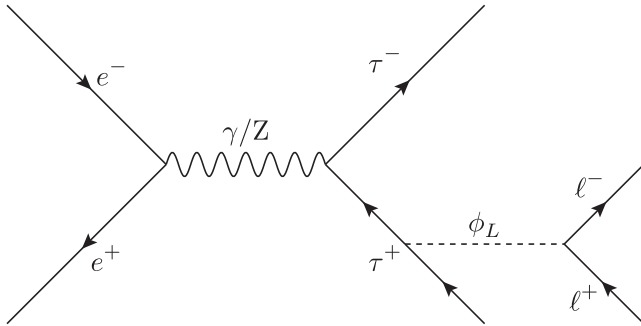

FIG. 1. Dominant Feynman diagram for production of ϕ_L in association with $\tau^+\tau^-$ pair in e^+e^- annihilation.

energy 60 MeV below the resonance. The luminosity values are measured with a relative systematic uncertainty of 1.4% [19]. The $e^+e^- \to q\bar{q}$ (where $q = u, d, s$, or c), and $e^+e^- \to B\bar{B}$ Monte Carlo (MC) samples are generated with EvtGen [20]. The $e^+e^- \to e^+e^-$ and $e^+e^- \to e^+e^-(\ell^+\ell^-/q\bar{q})$ (two-photon) samples are generated using BHLUMI [21] and AAFHB [22], respectively. We use KKMC [23] to generate $e^+e^- \to \mu^+\mu^-$ and $e^+e^- \to \tau^+\tau^-$ processes, and TAUOLA [24] to subsequently decay the τ leptons. Final state radiation is modeled with PHOTOS [25]. The signal process, $e^+e^- \to \tau^+\tau^-\phi_L$, $\phi_L \to \ell^+\ell^-$, is generated by a new feature of PHOTOS++ [26] integrated into KKMC. The signal cross sections are calculated using MadGraph5 [27], with initial state radiation modeled using the MGISR plugin [28]. The background cross sections are calculated with the respective generators, except for KKMC, for which results from [29] are used. The detector simulations and reconstructions are performed with GEANT3 [30] and BASF [31], respectively.

An important aspect of this analysis, in which it differs from the previous search performed by the *BABAR* experiment [32], is background modeling using MC samples and data in control regions. We use the multivariate analysis technique to enhance the presence of the signal over the background, as well as to define control regions, corresponding to regions enriched with each background component. The normalizations of the backgrounds are obtained by fitting the different MC components to data in different control regions. Studies of e^+e^- and $\mu^+\mu^-$ invariant masses as the discriminating variables are carried out by blinding the signal region until the optimization of the selection criteria is complete. In the final set of fits in the signal region, a uniform shape with Poisson fluctuations is added as an additional component to account for background from the unsimulated SM four-lepton processes $e^+e^- \to \tau^+\tau^-e^+e^-$ and $e^+e^- \to \tau^+\tau^-\mu^+\mu^-$.

We look for events with four tracks, each selected with a systematic uncertainty on the tracking efficiency of 0.35% [19]. To suppress misreconstructed and beam-induced tracks, we require the transverse (dr) and longitudinal ($|dz|$) projection of the distances of the closest approach to the interaction point be smaller than 10 and 50 mm, respectively. This selection criteria probes the parameter space with $\xi \sim 1$, which corresponds to a decay length of ϕ_L less than ~ 10 mm. For the $m_{\phi_L} < 0.1$ GeV region, decay lengths can be larger than 10 mm. In such cases, we require looser criteria of $dr < 50$ mm and $|dz| < 50$ mm.

The net charge of the event is required to be zero. In the $\phi_L \to e^+e^-$ ($\mu^+\mu^-$) channel, we require at least one track to be identified as e^+ (μ^+) and one track to be identified as e^- (μ^-) by our particle identification (PID) system. Correction factors for efficiency and the misidentification rates are obtained using control samples from data, and applied to MC samples. The precision of these correction factors is included as a systematic uncertainty.

We reconstruct ϕ_L candidates by fitting each pair of e^+e^- or $\mu^+\mu^-$ to a common vertex, while the remaining tracks in the event come from one-prong decays of the two τ leptons. Between 25% and 50% of the signal events have more than one ϕ_L candidate, with the average multiplicity decreasing from 1.7 to 1.3 at higher m_{ϕ_L} values. We choose the candidate with the smallest opening angle in the laboratory frame to ensure there is exactly one ϕ_L per selected event. The efficiency to select the true ϕ_L candidate per signal event is more than 98% (83%) for $\phi_L \to e^+e^-$ ($\mu^+\mu^-$) channel.

The major background for $\phi_L \to e^+e^-$ search comes from $e^+e^- \to \tau^+\tau^-$ events, where one of the $\tau^\pm$ leptons decays into a $\rho^\pm$ producing a π^0, which decays into $e^+e^-\gamma$ final state, thereby faking the event topology of the signal. The major background for $\phi_L \to \mu^+\mu^-$ search till $m_{\phi_L} = 1$ GeV comes from $e^+e^- \to \tau^+\tau^-$ events, where one of the $\tau^\pm$ leptons decay contains three charged pions, some of which are misidentified as muons. Beyond $m_{\phi_L} = 1$ GeV, the two muons mostly come from semileptonic decays of heavy quarks in $e^+e^- \to q\bar{q}$ events.

To suppress most of the Bhabha, $\mu^+\mu^-$ and two-photon backgrounds, we use rectangular selection criteria on the two-dimensional plane: $M_{\rm miss} \in [2, 6]$ GeV and $\theta_{\rm miss}^{\rm CM} \in [30°, 150°]$, where the missing mass ($M_{\rm miss}$) is evaluated using the four tracks and all neutrals detected in the final state, and $\theta_{\rm miss}^{\rm CM}$ is the polar angle of the missing momentum in the c.m. frame.

To suppress the remaining backgrounds, we train a multiclass boosted decision tree (BDT) for each channel, using the GradientBoostingClassifier model available in SCIKIT-LEARN [33]. We define five BDT scores to discriminate between the signal and four different types of backgrounds: $\tau^+\tau^-$, e^+e^- ($\mu^+\mu^-$), $q\bar{q}$, and $B\bar{B}$ in $\phi_L \to e^+e^-$ ($\phi_L \to \mu^+\mu^-$) channel.

The top four variables ranked according to their feature importance in the BDT for the $\phi_L \to e^+e^-$ channel are the thrust in the c.m. frame [34], the opening angle between the daughters of ϕ_L candidate in the laboratory frame, $M_{\rm miss}$ and the transverse distance of the vertex of the ϕ_L candidate from the interaction point. The top four variables for the $\phi_L \to \mu^+\mu^-$ channel are the invariant mass of τ^+ and τ^- daughter tracks, thrust, $M_{\rm miss}$ and the total energy of the reconstructed ϕ_L candidate in the laboratory frame. The other variables used in the BDT are event shapes (ratios of Fox-Wolfram moments [35]), missing particles (visible energy and direction of missing momentum in the c.m. frame), ϕ_L candidate (transverse momentum of daughter particles), PID (number of leptons, pion-kaon discriminator for ϕ_L daughters), neutral activity (number of π^0, the sum of energy deposited in ECL not associated with a track), and invariant mass of the system formed by the ϕ_L candidate and its nearest photon.

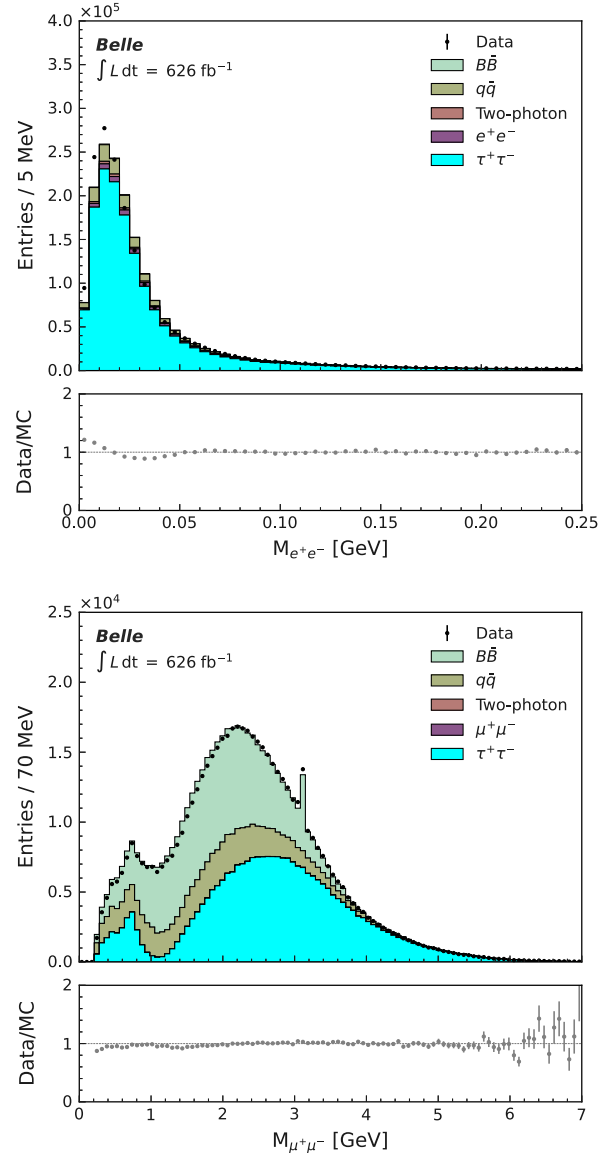In order to understand the background processes, we define the general control region (GCR) with negligible

FIG. 2. Data and MC distributions of e^+e^- invariant mass for $\phi_L \to e^+e^-$ channel (top) and $\mu^+\mu^-$ invariant mass for $\phi_L \to \mu^+\mu^-$ channel (bottom) in the GCR. All corrections and scale factors are applied to the MC distributions, after normalizing them to the integrated luminosity of data.

signal contributions for each channel by requiring the signal score to be less than 0.5. The dilepton mass distributions in the GCRs are shown in Fig. 2. We obtain the scale factors for each background component via a simultaneous fit across both channels. In order to estimate the uncertainty of the scale factors, we define a special control region (SCR) for each of those four backgrounds by requiring the corresponding BDT score to be greater than 0.5. We take the difference between the scale factors obtained from GCR and SCR as the uncertainty of each background contribution, except for the two-photon background, where the uncertainty is purely statistical. For the dominant background processes of $\tau^+\tau^-$, the scale factor is
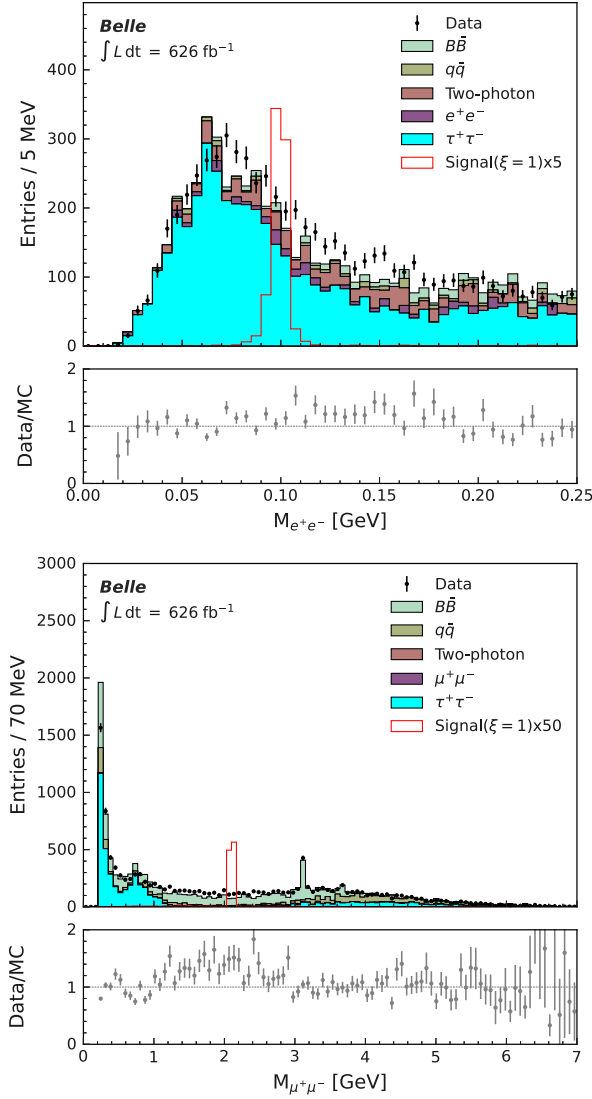
FIG. 4. e^+e^- invariant mass distributions are shown in the top subplot with 2.5 MeV bin width in the signal region corresponding to $m_{\phi_L} = 150$ MeV, which has the highest observed significance of 2.5 standard deviations in this channel. The data are shown as black dots, while the signal, $\tau^+\tau^-$, other Monte Carlo components of the backgrounds and the additional uniform background component are shown by pink, cyan, yellow, and green histograms, respectively. The statistical and systematic components of the uncertainty on total background have been added in quadrature and are shown by the shaded histogram. The bottom subplot compares the signal distribution with data minus the background contributions.

FIG. 3. Data and MC distributions of e^+e^- invariant mass for $\phi_L \to e^+e^-$ channel (top) and $\mu^+\mu^-$ invariant mass for $\phi_L \to \mu^+\mu^-$ channel (bottom) in SR. The MC are normalized to data, as in Fig. 2. The signal sample in $\phi_L \to e^+e^-$ ($\phi_L \to \mu^+\mu^-$) channel is generated with $m_{\phi_L} = 100$ MeV (2.1 GeV).

consistent with unity, with 6% (11%) relative uncertainty in e^+e^- ($\mu^+\mu^-$) channel.

We define the signal region (SR) with signal score >0.95 (0.65), as an optimum choice that maximizes the sensitivity for the e^+e^- ($\mu^+\mu^-$) channels, where the signal efficiency varies between 0.5% to 7.5% (5% to 17%). The distributions of e^+e^- and $\mu^+\mu^-$ invariant mass in SR are shown in Fig. 3, along with the MC backgrounds (stacked histograms) and signal distributions (red histograms). The ratio between the data and the sum of the MC backgrounds is shown at the bottom of each figure. No obvious narrow peak structure is observed, except for the J/ψ signal in the $\mu^+\mu^-$ channel. A slight excess of data above the MC samples in both channels is expected due to the above-mentioned unsimulated processes.
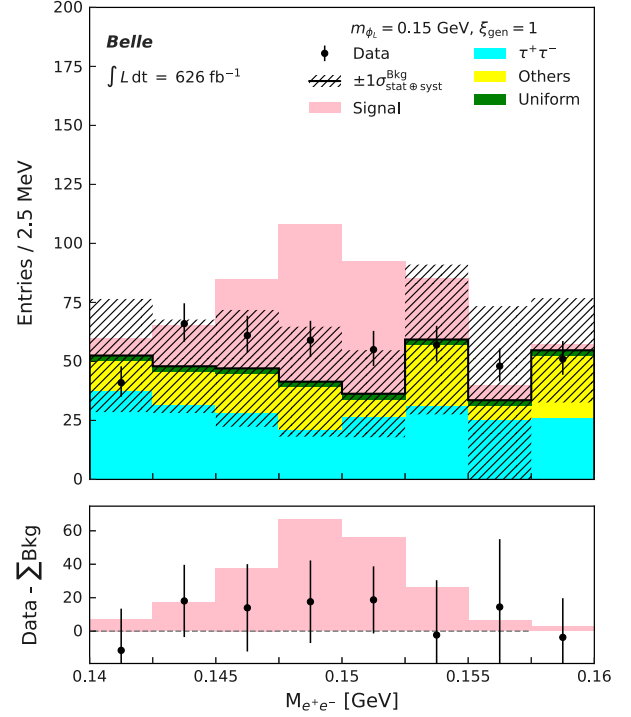
We search for narrow peaks in e^+e^- ($\mu^+\mu^-$) invariant mass distributions by performing binned maximum likelihood fits, where the likelihood is defined as a product of Possion distributions with expected events obtained from template histograms, and Gaussian distributions describing systematic uncertainties, as implemented in HistFactory [36]. We use one bin from $2m_e$ ($2m_\mu$) to $m_{\phi_L} - 2\sigma_{\phi_L}$, two to eight bins in $m_{\phi_L} \pm 2\sigma_{\phi_L}$ window, and one bin from $m_{\phi_L} + 2\sigma_{\phi_L}$ to 250 MeV (7 GeV). Here σ_{ϕ_L} is the resolution of the $\ell^+\ell^-$ mass distribution for the signal, and it varies in the [5, 30] MeV range, increasing at larger values of m_{ϕ_L}. The mass of ϕ_L is kept fixed in the fit and scanned from 40 to 210 MeV at 10 MeV intervals for e^+e^- channel, and from 225 MeV to 6.5 GeV at 25 MeV intervals for the $\mu^+\mu^-$ channel. We skip the ± 50 MeV window around the nominal mass of J/ψ and $\psi(2S)$, where we expect peaking backgrounds. The fit includes systematic uncertainties from luminosity, tracking efficiency, momentum scale, and PID corrections of ϕ_L daughter tracks, scale factors, and
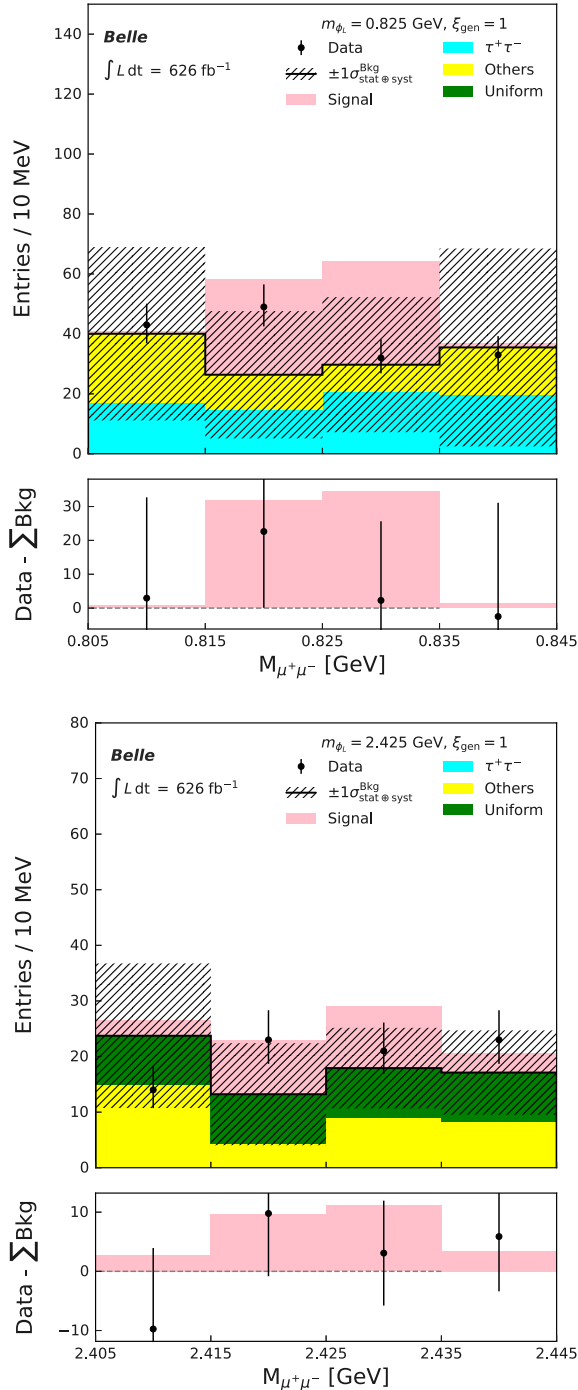
FIG. 5. $\mu^+\mu^-$ invariant mass distributions are shown in the top inset with 10 MeV bin width in the signal region corresponding to $m_{\phi_L} = 0.825$ and 2.425 GeV, which have the second highest and highest observed significance of 2.1 and 2.2 standard deviations in this channel, respectively. The data are shown as black dots, while the signal, $\tau^+\tau^-$, other Monte Carlo components of the backgrounds and the additional uniform background component are shown by pink, cyan, yellow, and green histograms, respectively. The statistical and systematic components of the uncertainty on total background have been added in quadrature and are shown by the shaded histogram. The bottom subplots compare the signal distribution with data minus the background contributions.
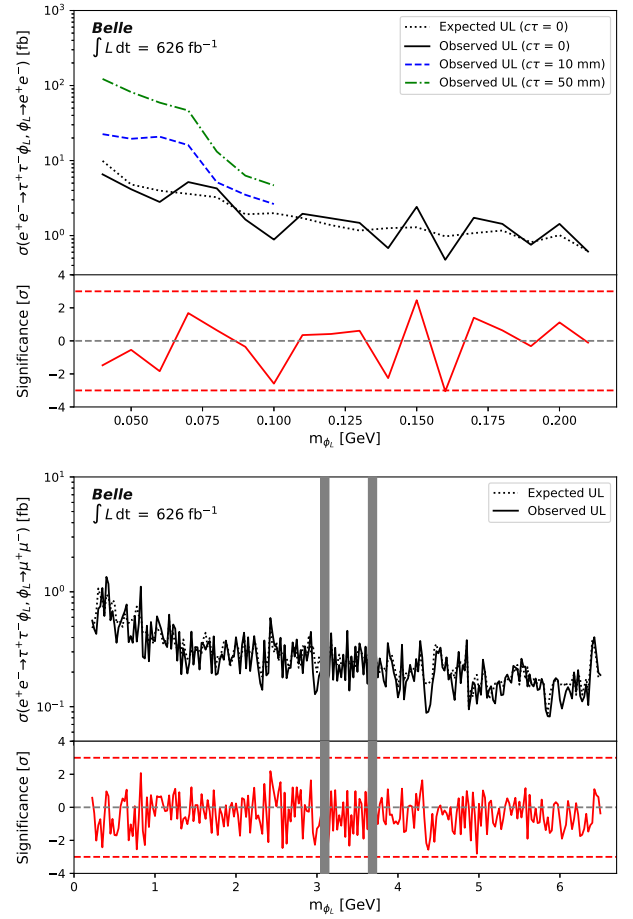

FIG. 6. Observed upper limits at 90% CL on the signal cross-section with mean proper decay lengths ($c\tau$) of 0, 10, and 50 mm, respectively, are shown in the top subplots as a function of the dark leptophilic scalar mass for $\phi_L \rightarrow e^+e^-$ channel (top) and $\phi_L \rightarrow \mu^+\mu^-$ channel (bottom). The bottom sub-plots in both of the figures show the observed significance for each channel. See text for details.
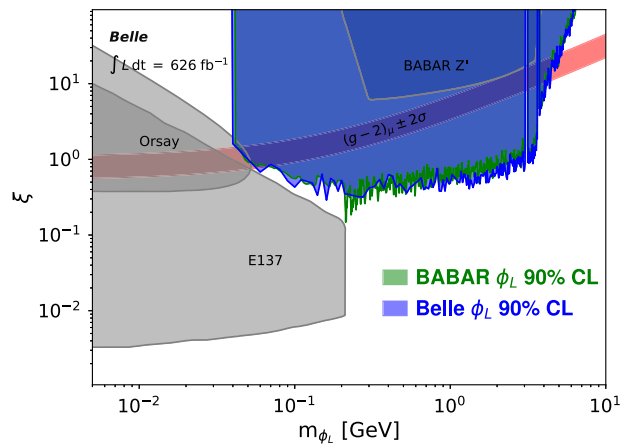

FIG. 7. Observed upper limits at 90% CL on the coupling constant ξ as a function of the ϕ_L mass from our search (blue), overlaid with results from *BABAR* (green) [32] and other searches (gray) [43–45]. The parameter space preferred by the $(g-2)_\mu$ measurement [2] is shown as a red band.

TABLE I. Observed upper limits at 90% CL on the coupling constant ξ as a function of the dark scalar mass.

m_{ϕ_L} [GeV]	$\xi_{\mathrm{obs}}^{\mathrm{UL}}$	m_{ϕ_L} [GeV]	$\xi_{\mathrm{obs}}^{\mathrm{UL}}$	m_{ϕ_L} [GeV]	$\xi_{\mathrm{obs}}^{\mathrm{UL}}$	m_{ϕ_L} [GeV]	$\xi_{\mathrm{obs}}^{\mathrm{UL}}$	m_{ϕ_L} [GeV]	$\xi_{\mathrm{obs}}^{\mathrm{UL}}$
0.040	1.610	1.100	0.528	2.425	1.169	3.950	6.882	5.275	27.814
0.050	1.000	1.125	0.506	2.450	1.017	3.975	6.742	5.300	28.678
0.060	0.680	1.150	0.492	2.475	0.909	4.000	5.958	5.325	34.832
0.070	0.860	1.175	0.690	2.500	0.907	4.025	6.761	5.350	36.915
0.080	0.740	1.200	0.495	2.525	0.817	4.050	11.036	5.375	35.949
0.090	0.520	1.225	0.640	2.550	1.014	4.075	6.652	5.400	35.807
0.100	0.430	1.250	0.621	2.575	0.687	4.100	8.289	5.425	43.741
0.110	0.539	1.275	0.456	2.600	0.963	4.125	8.929	5.450	44.129
0.120	0.512	1.300	0.616	2.625	0.698	4.150	10.629	5.475	44.814
0.130	0.486	1.325	0.408	2.650	0.782	4.175	10.067	5.500	40.440
0.140	0.335	1.350	0.534	2.675	0.791	4.200	9.697	5.525	52.190
0.150	0.642	1.375	0.485	2.700	1.033	4.225	12.562	5.550	49.473
0.160	0.289	1.400	0.425	2.725	0.907	4.250	11.485	5.575	50.988
0.170	0.560	1.425	0.481	2.750	1.088	4.275	16.106	5.600	42.933
0.180	0.516	1.450	0.663	2.775	0.863	4.300	14.171	5.625	49.827
0.190	0.380	1.475	0.482	2.800	1.003	4.325	10.710	5.650	46.459
0.200	0.530	1.500	0.581	2.825	0.802	4.350	8.647	5.675	46.820
0.210	0.351	1.525	0.586	2.850	1.060	4.375	9.011	5.700	51.991
0.225	0.343	1.550	0.474	2.875	0.930	4.400	9.983	5.725	47.706
0.250	0.323	1.575	0.627	2.900	1.042	4.425	12.643	5.750	49.518
0.275	0.317	1.600	0.623	2.925	1.268	4.450	14.789	5.775	56.750
0.300	0.418	1.625	0.599	2.950	0.860	4.475	18.627	5.800	55.059
0.325	0.438	1.650	0.644	2.975	0.697	4.500	18.769	5.825	43.879
0.350	0.539	1.675	0.669	3.000	0.728	4.525	20.492	5.850	42.688
0.375	0.416	1.700	0.489	3.025	0.858	4.550	17.201	5.875	44.020
0.400	0.629	1.725	0.717	3.150	0.912	4.575	17.250	5.900	53.655
0.425	0.599	1.750	0.492	3.175	1.412	4.600	20.211	5.925	67.005
0.450	0.424	1.775	0.504	3.200	0.892	4.625	16.634	5.950	71.073
0.475	0.475	1.800	0.584	3.225	1.243	4.650	18.014	5.975	71.839
0.500	0.420	1.825	0.626	3.250	0.904	4.675	16.081	6.000	61.226
0.525	0.359	1.850	0.597	3.275	1.072	4.700	14.723	6.025	58.011
0.550	0.425	1.875	0.733	3.300	0.959	4.725	19.830	6.050	65.471
0.575	0.453	1.900	0.667	3.325	1.221	4.750	25.134	6.075	74.199
0.600	0.490	1.925	0.595	3.350	0.953	4.775	18.791	6.100	79.979
0.625	0.524	1.950	0.641	3.375	1.585	4.800	23.124	6.125	79.262
0.650	0.572	1.975	0.654	3.400	0.880	4.825	22.510	6.150	77.155
0.675	0.398	2.000	0.802	3.425	1.257	4.850	31.242	6.175	104.137
0.700	0.430	2.025	0.706	3.450	1.029	4.875	16.014	6.200	88.988
0.725	0.409	2.050	0.570	3.475	1.422	4.900	18.705	6.225	115.162
0.750	0.543	2.075	0.767	3.500	1.116	4.925	22.153	6.250	92.529
0.775	0.426	2.100	0.876	3.525	1.504	4.950	22.205	6.275	91.434
0.800	0.516	2.125	0.618	3.550	1.394	4.975	18.850	6.300	100.179
0.825	0.759	2.150	0.855	3.575	1.314	5.000	23.159	6.325	118.988
0.850	0.382	2.175	0.616	3.600	2.211	5.025	21.628	6.350	100.772
0.875	0.380	2.200	0.735	3.625	1.877	5.050	31.480	6.375	146.809
0.900	0.536	2.225	0.893	3.750	3.806	5.075	28.369	6.400	202.637
0.925	0.380	2.250	0.765	3.775	5.047	5.100	22.649	6.425	231.121
0.950	0.571	2.275	0.659	3.800	4.989	5.125	25.092	6.450	205.183
0.975	0.483	2.300	0.573	3.825	4.700	5.150	26.815	6.475	180.166
1.000	0.483	2.325	0.544	3.850	4.740	5.175	23.824	6.500	185.935
1.025	0.628	2.350	0.902	3.875	7.846	5.200	23.664		
1.050	0.598	2.375	0.643	3.900	7.309	5.225	29.744		
1.075	0.569	2.400	0.666	3.925	7.322	5.250	31.265		

selection efficiency of BDT. To account for the unsimulated processes, we include an additional uniform background component.

We use the profile likelihood ratio as the test statistic [37] to compare data with signal-plus-background or background-only hypothesis. The fraction of each background component and the additional uniform component are allowed to vary within their uncertainties. The fit returns the signal yield as well as the normalization factor for each background component, along with the nuisance parameters describing systematic uncertainties. In order to obtain the signal significance, we first calculate the p value, the probability that the data is explained as the statistical fluctuation of the background. We then calculate the signed significance, where the sign follows the convention elaborated in Ref. [38]. The signal significances are shown in the bottom subplots in Fig. 6 for e^+e^- (top) and $\mu^+\mu^-$ (bottom) channels. We find all the mass points have significance less than three standard deviations (σ). Fit results for three mass points ($m_{\phi_L} = 0.15$, 0.825, and 2.425 GeV) with significance more than 2σ are shown in Figs. 4 and 5.

To enable direct comparison with existing upper limits (UL) from the *BABAR* experiment [32], we calculate Bayesian UL using the Metropolis-Hastings algorithm [39,40] as implemented in RooStats [41]. A toy Monte Carlo–based numerical integration technique [41] is used to cross check our Bayesian result, which agrees within a couple of percents across the whole mass range. The UL of the signal cross section at 90% confidence level (CL) [42] are shown in the top subplots in Fig. 6.

We also cross check our results using an alternate fitting method as used by *BABAR* experiment [32], where the background is modeled as a smooth polynomial from sideband data, and the signal is modeled as a Gaussian. The observed significance from these two methods agree within 0.35σ on the average.

Both the cross section and the proper decay length ($c\tau$) of the dark leptophilic scalar depend on the coupling constant ξ. For $m_{\phi_L} > 0.1$ GeV, the obtained UL on ξ is consistent with the assumption that $c\tau$ is short enough to have negligible influence on the signal detection efficiency. However, for $m_{\phi_L} < 0.1$ GeV, $c\tau$ of ~ 10 to 50 mm is expected for $\xi \sim 1$. To take this dependence into account, we simulate the events with two additional values of $c\tau = 10$ mm and $c\tau = 50$ mm, and reperform the entire analysis to determine the UL on the cross section for these values. Using these UL and the known relation between $c\tau$ and ξ, we iteratively determine the UL on the ξ, as shown in the top subplot of Fig. 6.

The exclusion region of the coupling constant ξ vs m_{ϕ_L} is shown in Fig. 7, overlaid with previous results [32,43–45]. Our limits are tabulated in Table I.

A fit to the ratio of limits obtained by the *BABAR* experiment [32] and our limits show that our results are more constraining by 19% on the average. We exclude the parameter space with m_{ϕ_L} between [0.04, 4] GeV favored by $(g-2)_\mu$ at 90% CL [10, 11].

In conclusion, we search for a dark leptophilic scalar and set the UL on the cross section of $e^+e^- \to \tau^+\tau^-\phi_L$, $\phi_L \to e^+e^-$ process in the range [0.6, 7] fb and on the cross section of $e^+e^- \to \tau^+\tau^-\phi_L$, $\phi_L \to \mu^+\mu^-$ process in the range [0.1, 2] fb at 90% CL. There is no such leptophilic scalar with mass less than 4 GeV that can explain the observed excess in $(g-2)_\mu$.

[1] E. Corbelli and P. Salucci, Mon. Not. R. Astron. Soc. **311,** 441 (2000).

[2] B. Abi *et al.* (Muon $g-2$ Collaboration), Phys. Rev. Lett. **126,** 141801 (2021).

[3] P. J. Fox and E. Poppitz, Phys. Rev. D **79,** 083528 (2009).

[4] C.-Y. Chen, H. Davoudiasl, W. J. Marciano, and C. Zhang, Phys. Rev. D **93,** 035006 (2016).

[5] D. Abercrombie *et al.*, Phys. Dark Universe **27,** 100371 (2020).

[6] J. Beacham *et al.*, J. Phys. G **47,** 010501 (2020).

[7] G. C. Branco, P. M. Ferreira, L. Lavoura, M. N. Rebelo, M. Sher, and J. P. Silva, Phys. Rep. **516,** 1 (2012).

[8] Y.-S. Liu, D. McKeen, and G. A. Miller, Phys. Rev. Lett. **117,** 101801 (2016).

[9] P. Agrawal, Z. Chacko, and C. B. Verhaaren, J. High Energy Phys. 08 (2014) 147.

[10] B. Batell, N. Lange, D. McKeen, M. Pospelov, and A. Ritz, Phys. Rev. D **95,** 075003 (2017).

[11] J. Liu, N. McGinnis, C. E. M. Wagner, and X.-P. Wang, J. High Energy Phys. 04 (**2020**) 197.

[12] L. Calibbi, A. Crivellin, and B. Zaldívar, Phys. Rev. D **92,** 016004 (2015).

[13] A. Crivellin, F. Kirk, C. A. Manzari, and L. Panizzi, Phys. Rev. D **103,** 073002 (2021).

[14] A. Freitas and S. Westhoff, J. High Energy Phys. 10 (2014) 116.

[15] Natural units ($\hbar = c = 1$) are used throughout this paper.

[16] K. Akai *et al.*, Nucl. Instrum. Methods Phys. Res., Sect. A **499,** 191 (2003).

[17] A. Abashian *et al.* (Belle Collaboration), Nucl. Instrum. Methods Phys. Res., Sect. A **479,** 117 (2002).

[18] R. Abe *et al.*, Nucl. Instrum. Methods Phys. Res., Sect. A **535,** 558 (2004).

[19] J. Brodzicka *et al.* (Belle Collaboration), Prog. Theor. Exp. Phys. **2012,** 04D001 (2012).

[20] D. J. Lange, Nucl. Instrum. Methods Phys. Res., Sect. A **462,** 152 (2001).

[21] S. Jadach, E. Richter-Was, B. F. L. Ward, and Z. Was, Comput. Phys. Commun. **70,** 305 (1992).

[22] F. A. Berends, P. H. Daverveldt, and R. Kleiss, Comput. Phys. Commun. **40,** 285 (1986).

[23] S. Jadach, B. F. L. Ward, and Z. Was, Comput. Phys. Commun. **130,** 260 (2000).

[24] S. Jadach, Z. Was, R. Decker, and J. H. Kühn, Comput. Phys. Commun. **76,** 361 (1993).

[25] E. Barberio and Z. Was, Comput. Phys. Commun. **79,** 291 (1994).

[26] S. Banerjee, D. Biswas, T. Przedzinski, and Z. Was, arXiv:2111.05914.

[27] J. Alwall, R. Frederix, S. Frixione, V. Hirschi, F. Maltoni, O. Mattelaer, H.-S. Shao, T. Stelzer, P. Torrielli, and M. Zaro, J. High Energy Phys. 07 (**2014**) 079.

[28] Q. Li and Q. Yan, arXiv:1804.00125.

[29] S. Banerjee, B. Pietrzyk, J. M. Roney, and Z. Was, Phys. Rev. D **77,** 054012 (2008).

[30] R. Brun, F. Bruyant, M. Maire, A. C. McPherson, and P. Zanarini, CERN Report No. DD/EE/84-1, 1987.

[31] R. Itoh, Comput. Phys. Commun. **110,** 1 (1998), https://inspirehep.net/literature/445749.

[32] J. P. Lees *et al.* (*BABAR* Collaboration), Phys. Rev. Lett. **125,** 181801 (2020).

[33] F. Pedregosa, G. Varoquaux, A. Gramfort *et al.*, J. Mach. Learn. Res. **12,** 2825 (2011), https://dl.acm.org/doi/10.5555/1953048.2078195.

[34] S. Brandt, C. Peyrou, R. Sosnowski, and A. Wroblewski, Phys. Lett. **12,** 57 (1964).

[35] G. C. Fox and S. Wolfram, Phys. Rev. Lett. **41,** 1581 (1978).

[36] K. Cranmer, G. Lewis, L. Moneta, A. Shibata, and W. Verkerke (ROOT Collaboration), Report No. CERN-OPEN-2012-016, 2012.

[37] G. Cowan, K. Cranmer, E. Gross, and O. Vitells, Eur. Phys. J. C **71,** 1554 (2011); **73,** 2501(E) (2013).

[38] G. Aad *et al.* (ATLAS Collaboration), Phys. Rev. D **86,** 032003 (2012).

[39] N. Metropolis, A. W. Rosenbluth, M. N. Rosenbluth, A. H. Teller, and E. Teller, J. Chem. Phys. **21,** 1087 (1953).

[40] W. K. Hastings, Biometrika **57,** 97 (1970).

[41] L. Moneta, K. Belasco, K. S. Cranmer, S. Kreiss, A. Lazzaro, D. Piparo, G. Schott, W. Verkerke, and M. Wolf, Proc. Sci. ACAT2010 (**2010**) 057 [arXiv:1009.1003].

[42] As we use the Bayesian method, this is *credibility level* but we use *confidence level* here following common convention.

[43] J. P. Lees *et al.* (*BABAR* Collaboration), Phys. Rev. D **94,** 011102 (2016).

[44] J. D. Bjorken, S. Ecklund, W. R. Nelson, A. Abashian, C. Church, B. Lu, L. W. Mo, T. A. Nunamaker, and P. Rassmann, Phys. Rev. D **38,** 3375 (1988).

[45] M. Davier and H. Nguyen, Phys. Lett. B **229,** 150 (1989).